IGBT Temperature Field Monitoring Based on Reduced-order Model

Ziyu Zhou, Yi Sui, *Member, IEEE*, Xu Zhang, Chengde Tong, *Member, IEEE*, Ping Zheng, *Senior Member, IEEE*, and Mingjun Zhu

***Abstract*—With the rapid development of the world economy, IGBT has been widely used in motor drive and electric energy conversion. In order to timely detect the fatigue damage of IGBT, it is necessary to monitor the junction temperature of IGBT. In order to realize the fast calculation of IGBT junction temperature, a finite element method of IGBT temperature field reduction is proposed in this paper. Firstly, the finite element calculation process of IGBT temperature field is introduced and the linear equations of finite element calculation of temperature field are derived. Temperature field data of different working conditions are obtained by finite element simulation to form the sample space. Then the covariance matrix of the sample space is constructed, whose proper orthogonal decomposition and modal extraction are carried out. Reasonable basis vector space is selected to complete the low dimensional expression of temperature vector inside and outside the sample space. Finally, the reduced-order model of temperature field finite element is obtained and solved. The results of the reduced order model are compared with those of the finite element method, and the performance of the reduced-order model is evaluated from two aspects of accuracy and rapidity.**

***Index Terms*—IGBT Junction temperature, Proper orthogonal decomposition, Reduced-order model.**

I. Introduction

With the rapid development of the world economy, IGBT is more and more widely used in motor drive and electric energy conversion. The safe operation of IGBT is becoming more and more important. The state monitoring of the system has become the focus of reliability research. According to the stress analysis of IGBT, too high junction temperature amplitude or too large junction temperature fluctuation is the main cause of internal fatigue damage and even failure of power devices [1]-[2], thus affecting system reliability.

In order to evaluate the fatigue damage of IGBT and predict its life in time, real-time monitoring of IGBT junction temperature is necessary. However, in the IGBT package structure, semiconductor chips are usually placed inside the device module, so it is difficult to measure the junction temperature directly. Therefore, scholars have proposed a variety of methods to measure and calculate the junction temperature of IGBT.

In order to directly study the nodal temperature variation of IGBT, some scholars adopted direct measurement methods, including contact method and radiation temperature measurement [3]-[5]. The contact method is to measure the junction temperature of the power device by removing the thermal sensitive element directly from the surface of the semiconductor chip inside the power device. Radiation temperature measurement method refers to the use of infrared thermal imager to photograph the chip layer surface, so as to obtain the power module chip layer two-dimensional temperature distribution image. However, this direct measurement method is limited by the internal structure of IGBT, which is difficult to be applied in engineering due to insufficient contact between temperature sensitive elements and chip and inaccurate material emissivity.

In addition to direct measurement, calculation methods are also commonly used to obtain IGBT junction temperature, mainly including thermal network model method and finite element calculation method. The thermal network model method is equivalent to the thermal resistance and heat capacity network, and the junction temperature is calculated by using the power loss and shell temperature of the power device. This method is quick in calculation, but it needs accurate measurement or parameter identification of heat resistance and heat capacity [6]-[8]. In the finite element calculation of IGBT junction temperature, IGBT power loss should be used as the heat source for electrothermal co-simulation [9]. This method can accurately calculate the temperature field of IGBT module. However, the large amount of calculation and long time of finite element calculation are not conducive to real-time monitoring of IGBT junction temperature and digital twin application [10]-[11].

In order to improve the speed and accuracy of IGBT temperature monitoring model, this paper studies the reduced-order method of IGBT temperature field finite element

Manuscript received March 02, 2022; revised March 09, 2022; accepted March 17, 2022. Date of publication June 25, 2023; Date of current version January 11, 2023.

This work was supported in part by Heilongjiang Provincial Natural Science Foundation of China under Project TD2021E004, and in part by Ningbo Science and Technology Bureau under S&T Innovation 2025 Major Special Programme with project code 2019B10071. *(Corresponding Author: Ziyu Zhou)*

Ziyu Zhou, Yi Sui, Xu Zhang, Chengde Tong and Ping Zheng are with School of Electrical Engineering & Automation, Harbin Institute of Technology, Harbin 150001, China (e-mail: zyzhou_hit@163.com; suiyi @hit.edu.cn; zhangxu_97930@163.com; tongchengde@hit.edu.cn; zhengping@hit.edu.cn).

Mingjun Zhu is with Flight control department, Xi'an Flight Automatic Control Research Institute, Xi'an 710076, China (e-mail: woshizhumingjun@126.com).

Digital Object Identifier 10.30941/CESTEMS.2023.00005

model on the basis of IGBT temperature field simulation calculation.

In this paper, the IGBT thermal steady-state finite element model is firstly established. Then the modal extraction of temperature field sample space is carried out by using the proper orthogonal decomposition. The finite element model of temperature field is simplified to carry out the rapid calculation of temperature field, and the effectiveness of the reduced-order model is evaluated.

II. Reduced-order model of IGBT Module Temperature Field

A. Proper Orthogonal Decomposition of Finite Element Model of IGBT Temperature Field

In the finite element calculation of IGBT temperature field, the partial differential equation of transient heat conduction problem needs to be written according to IGBT internal heat source and convective boundary conditions, and the boundary conditions are given. Next, the solution domain is discretized into finite subdomains according to the segmented grid [12]-[13]. Then Galerkin method is used to construct the finite element form of the steady-state heat conduction problem which is transformed into linear equations to solve the variable values of each grid node, as in (1),

$$\boldsymbol{KT} = \boldsymbol{L} \tag{1}$$

where $\boldsymbol{K}$ is the $m\times m$ stiffness matrix, including heat conduction matrix $\boldsymbol{K}1$ and convection matrix $\boldsymbol{H}$, which is composed of heat conduction matrix and convection matrix. It represents the heat transfer performance of IGBT, and is only related to the material properties and division mode. $\boldsymbol{L}$ is the load matrix, including the heat source vector $\boldsymbol{G}$ and the heat flux vector $\boldsymbol{F}$, which consists of heat source vector and heat flux vector, and mainly reflects the heat source of IGBT. $\boldsymbol{K}$ and $\boldsymbol{L}$ are shown in (2) and (3),

$$\boldsymbol{K} = \boldsymbol{K}_1 + h\boldsymbol{K}_2 \tag{2}$$

$$\boldsymbol{L} = Q\boldsymbol{L}_1 + hT_{\text{ext}}\boldsymbol{L}_2 \tag{3}$$

where $h\boldsymbol{K}2$, QL1 and $hT_{\text{ext}}\boldsymbol{L}_2$ are convection matrix $\boldsymbol{H}$, the heat source vector $\boldsymbol{G}$ and the heat flux vector $\boldsymbol{F}$. By solving the linear equations, the temperature of each network node can be obtained and the temperature distribution of IGBT can be obtained[14].

The dimension of the general finite element equations is large, and it takes a long time to directly solve the linear equations. Therefore, the proper orthogonal decomposition method can be used to build the reduced-order model to improve the calculation efficiency.

Proper orthogonal decomposition is a common data dimension reduction method, whose basic principle is as follows: Suppose that a function or physical field vector space U(x) can be approximated by an orthogonal basis, as in (4), where $\varphi_i(x)$ is the basis function or basis vector.

$$U(x) = \sum_{i=1}^{n} \eta_i \varphi_i(x) \tag{4}$$

$$U'(x) = \sum_{i=1}^{r} \eta_i \varphi_i(x) \tag{5}$$

The purpose of the proper orthogonal decomposition is to find a set of orthogonal basis function best on U(x) or base vector approximation, so need to get U(x) of a part of the sample data, the sample space is usually expressed as the form of matrix, which is also called the snapshot matrix, each column in the sample space the number a moment or a condition of the physical fields at different spatial location of the data. To solve the eigenvalue problem based on the sample data, the eigenvalue represents the energy of the physical field contained in the corresponding mode. The obtained modes are sorted in descending order according to the eigenvalue, and the modes of the first order r are selected for approximation. The original function or the vector space U(x) of the physical field can be expressed as in (5). The specific implementation process of the intrinsic orthogonal decomposition method is shown in Fig. 1.

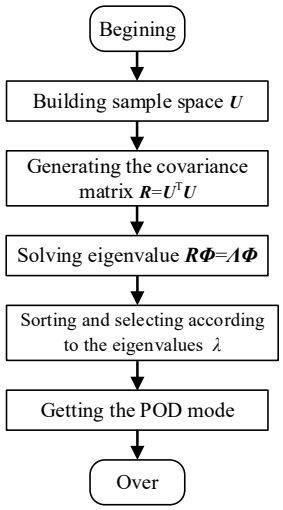

Fig. 1. The flow of proper orthogonal decomposition method.

Taking Infineon-FS200R07A5E3 IGBT of Infineon as reference, the thermal model of IGBT module is established in COMSOL Multiphysics. The top surface of the module is set as adiabatic boundary condition. Considering the role of radiator, the bottom surface of the module is defined as convective heat flux boundary condition, which includes heat transfer coefficient h and external temperature T_{ext}. When the module is used as an inverter, the power loss is evenly distributed among the chips, assuming that the power loss Q is evenly distributed among the chips.

$$\boldsymbol{U} = \begin{pmatrix} T_1(\boldsymbol{w}_1) & T_1(\boldsymbol{w}_2) & \cdots & T_1(\boldsymbol{w}_n) \\ T_2(\boldsymbol{w}_1) & T_2(\boldsymbol{w}_2) & \cdots & \cdots \\ \cdots & \cdots & T_i(\boldsymbol{p}_j) & \cdots \\ T_m(\boldsymbol{w}_1) & T_m(\boldsymbol{w}_2) & \cdots & T_m(\boldsymbol{w}_n) \end{pmatrix} \tag{6}$$

It is defined that parameter vector $\boldsymbol{w}$ contains the total power loss Q and heat transfers coefficient h of IGBT module, which is $\boldsymbol{w}=(h,Q)$, representing the operating conditions of IGBT module. The sample space $\boldsymbol{U}$ of IGBT module temperature field is shown in (6), which is composed of temperature data of m nodes and n operating conditions. The temperature field data of each column of matrix $\boldsymbol{U}$ when the parameter vector is fixed. Each element $T_i(\boldsymbol{w}_j)$ in the matrix is the node temperature numbered i under the working conditions defined by $\boldsymbol{w}_j$.

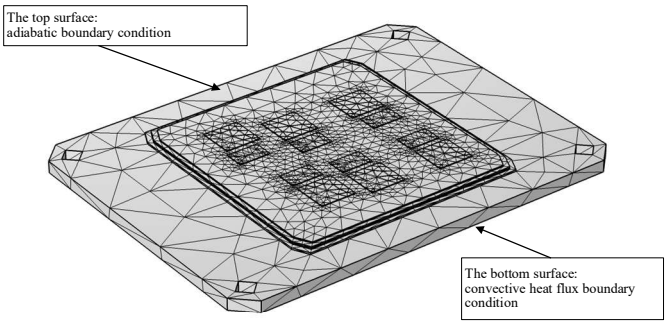

Fig. 2. IGBT module finite element analysis results.

The geometric model of IGBT module is divided into grids, which contain 2770 node positions in total, as in Fig. 2.

12 groups of working conditions as in Fig. 3 are selected for finite element simulation. The sample space is consist of simulation results.

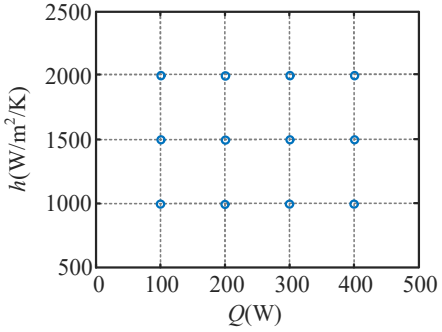

Fig. 3. Sample space composition.

In order to extract the basis vectors that can effectively represent the sample space $\boldsymbol{U}$, proper orthogonal decomposition is performed on the vector space. The matrix $\boldsymbol{U}$ is not a square matrix. The covariance matrix, as in (7), is formed by multiplying the matrix $\boldsymbol{U}$ and its transpose matrix $\boldsymbol{U}^{\mathrm{T}}$

$$\boldsymbol{U}\boldsymbol{U}^{\mathrm{T}}\boldsymbol{\Phi} = \boldsymbol{\Lambda}\boldsymbol{\Phi} \tag{7}$$

where $\boldsymbol{\Phi}$ is Eigenvector matrix, $\boldsymbol{\Phi} = (\boldsymbol{\varphi}_1, \boldsymbol{\varphi}_2, \ldots, \boldsymbol{\varphi}_m)$, $\boldsymbol{\Lambda}$ is angular matrix of diagonal elements with eigenvalues, $\boldsymbol{\Lambda} = diag(\lambda_1, \lambda_2, \ldots, \lambda_m)$. M eigenvalues and eigenvectors can be obtained by solving the eigenvalue problem of the covariance matrix.

After the proper orthogonal decomposition of the signal, the magnitude of the eigenvalue represents the magnitude of the signal energy contained in the mode [15]. M eigenvalues are sorted in descending order, and m eigenvectors are sorted in order of eigenvalues. Generally, the first several eigen roots are much larger than the latter, which means that the first several modes can contain most of the energy of the signal, which is enough to summarize the characteristics of the whole signal and restore the original matrix. In order to select as few modes as possible to approximate the original matrix, the relative energy of each mode can be calculated according to (8).

$$E_i = \frac{\lambda_i}{\sum_{k=1}^{m}\lambda_k} \quad (i = 1, 2, ..., m) \tag{8}$$

Proper orthogonal decomposition is carried out on the sample space. The eigenvalues are arranged in descending order, and the relative energy of each mode is calculated. The relative energy curves of the first 15 orders are drawn in Fig. 4.

It can be seen that the relative energy of each mode gradually decreases, and the relative energy of the first four modes is relatively large.

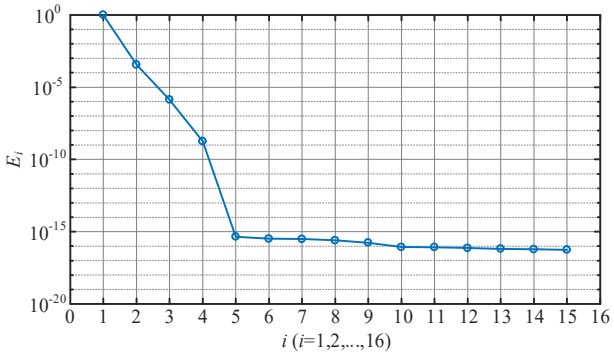

Fig. 4. The relative energy ratio of the first 15 modes.

Table I lists the eigenvalues of the first 6 modes, as well as the sum of the relative and cumulative energies of each mode.

TABLE I
EIGENVALUES AND ENERGY RATIOS OF THE FIRST 6 MODES AND CUMULATIVE RNERGY RATIOS

i	Eigenvalue λ_i	Energy ratio E_i	Cumulative energy ratio $\sum_{k=1}^{i} E_k$
1	1.72e08	0.99964	0.999636
2	6.23e04	0.00036	0.999998
3	2.36e02	1.37e-06	0.999999
4	0.31	1.78e-09	1.000000
5	8.05e-08	4.68e-16	1.000000
6	6.89e-08	4.00e-16	1.000000

When selecting modes, the principle of $E_i \geq 10^{-10}$ is adopted. Therefore, the first four modes can be selected for approximate reduction of sample space $\boldsymbol{U}$. According to Table I, the sum of the relative energy of the first four modes is very close to 1, which can summarize most features of the signal.

According to the principle of proper orthogonal decomposition, the snapshot matrix $\boldsymbol{U}$ can be decomposed into the product of the eigenvector matrix $\boldsymbol{\Phi}$ and the coefficient matrix $\boldsymbol{A}$, which is $\boldsymbol{U}=\boldsymbol{\Phi}\boldsymbol{A}$. Coefficient matrix $\boldsymbol{A}=[\boldsymbol{\alpha}(\boldsymbol{w}_1), \boldsymbol{\alpha}(\boldsymbol{w}_2), \ldots, \boldsymbol{\alpha}(\boldsymbol{w}_n)]$. Each column in the coefficient matrix of $\boldsymbol{\alpha}(\boldsymbol{p}_i)= [\boldsymbol{\alpha}_1(\boldsymbol{w}_i), \boldsymbol{\alpha}_2(\boldsymbol{w}_i), \ldots, \boldsymbol{\alpha}_m(\boldsymbol{w}_i)]^{\mathrm{T}}$, $i=1,2,\ldots,n$. Then each column vector $\boldsymbol{T}(\boldsymbol{w}_i)$ in snapshot matrix $\boldsymbol{U}$ can be decomposed into the product of feature vector matrix $\boldsymbol{\Phi}$ and coefficient vector $\boldsymbol{\alpha}_i$, as in (9).

$$\boldsymbol{T}(\boldsymbol{w}_i) = \sum_{j=1}^{m}\boldsymbol{\alpha}_j(\boldsymbol{w}_i)\boldsymbol{\varphi}_j = \boldsymbol{\Phi}\boldsymbol{\alpha}(\boldsymbol{w}_i) \tag{9}$$

Since the eigenvector matrix obtained by the proper orthogonal decomposition is orthogonal, the coefficient matrix $\boldsymbol{\alpha}(\boldsymbol{w}_i)$ of the temperature field $\boldsymbol{T}(\boldsymbol{w}_i)$ can be solved according to (10).

$$\boldsymbol{\alpha}(\boldsymbol{w}_i) = \boldsymbol{\Phi}^{-1}\boldsymbol{T}(\boldsymbol{w}_i) \tag{10}$$

The former mode of order r is selected to approximate the original temperature field data $\boldsymbol{T}(\boldsymbol{w}_i)$, and the approximate value $\boldsymbol{T}(\boldsymbol{w}_i)$ can be expressed as in (11), where $\boldsymbol{\Phi}_r$ is the eigenvector

matrix composed of the former r order eigenvectors, which is $\boldsymbol{\Phi}_r = (\boldsymbol{\varphi}_1, \boldsymbol{\varphi}_2, \ldots, \boldsymbol{\varphi}_r)$.

$$\boldsymbol{T}_r(\boldsymbol{w}_i) = \sum_{j=1}^{r} \boldsymbol{\alpha}_j(\boldsymbol{w}_i)\boldsymbol{\varphi}_j = \boldsymbol{\Phi}_r \boldsymbol{\alpha}_j(\boldsymbol{w}_i) \tag{11}$$

B. Construction and Solution of Reduced-order Model

The combination of proper orthogonal decomposition and Galerkin method can be used to construct a reduced-order model of sample space. First, the basis function or basis vector can be obtained by using the proper orthogonal decomposition. The quantities to be solved are expressed as linear combinations of basis functions or basis vectors as approximate solutions. In Galerkin method, the basis function or basis vector is also used to construct the weight function. The partial differential equation is multiplied by the weight function and integrated over the solution domain to obtain the weak solution form. By substituting the approximate solution and weight function into the weak solution form, the linear equations of the original problem can be obtained. The low-dimensional linear equations can be obtained by projecting the equations onto the subspace of the basis vectors obtained by the proper orthogonal decomposition. The dimension of the equations is independent of the mesh number, which is consistent with the modal number obtained by the proper orthogonal decomposition, and greatly reduced compared with the original equations. Finally, the specific steps of building the reduced-order model based on the proper orthogonal decomposition method are summarized as follows:

1) The temperature field data at m locations under n different working conditions are obtained through finite element simulation of the original model, which is used to form the sample space $\boldsymbol{U}$.

2) Calculate the covariance matrix $\boldsymbol{U}\boldsymbol{U}^{\mathrm{T}}$. By solving the (7), the eigenvalue $\lambda_i(i=1,2,\ldots,m)$ and the eigenvector $\boldsymbol{\varphi}_i$ $(i=1,2,\ldots,m)$, and then arrange them according to the order of eigenvalues from large to small;

3) The first r eigenvectors are selected as the basis vectors so that the first r modes contain almost all the energy of the signal.

4) The higher-order equations shown in (1) are projected onto the basis vectors to obtain the reduced-order equations. Then the numerical reduced-order model of the original finite element model can be obtained.

5) Assemble system matrix according to finite element theory. Solve the temperature field data.

After the construction of the reduced-order model is completed, the temperature field data can be quickly solved by solving the low-order equation. The specific method is as follows:

Equation (12) can be obtained by substituting (11) into (1).

$$\boldsymbol{K}\boldsymbol{\Phi}_r\boldsymbol{\alpha}(\boldsymbol{w}) = \boldsymbol{L} \tag{12}$$

For the working condition $\boldsymbol{w}$, which is not repeated with the 12 working conditions in the sample space, the temperature field data under the corresponding unknown working conditions can be obtained as long as $\boldsymbol{\alpha}(\boldsymbol{w})$ is solved. Equation (12) is composed of m equations and r unknowns. In order to eliminate redundant equations and determine the unique solution, multiply both sides of (12) by $\boldsymbol{\Phi}_r$ transpose, and substitute (2) and (3) into (12), and (13) can be obtained, where $\boldsymbol{K}_r$ and $\boldsymbol{L}_r$ can be obtained from (14) and (15) respectively.

$$\boldsymbol{K}_r\boldsymbol{\alpha}(\boldsymbol{w}) = \boldsymbol{L}_r \tag{13}$$

$$\boldsymbol{K}_r = \boldsymbol{\Phi}_r^{\mathrm{T}}\boldsymbol{K}_1\boldsymbol{\Phi}_r + h\boldsymbol{\Phi}_r^{\mathrm{T}}\boldsymbol{K}_2\boldsymbol{\Phi}_r \tag{14}$$

$$\boldsymbol{L}_r = Q\boldsymbol{\Phi}_r^{\mathrm{T}}\boldsymbol{L}_1 + hT_a\boldsymbol{\Phi}_r^{\mathrm{T}}\boldsymbol{L}_2 \tag{15}$$

Through the above transformation, the m-dimensional higher-order equations shown in (1) are transformed into the r-dimensional equations shown in the solution (12), so as to complete the reduced-order operation of the original finite element model. Because of $r << m$, solving (12) is much faster than solving (1).

III. Simulation and Performance Evaluation of Reduced-order Model

A. Reduced-order Model Simulation in Sample Space

Fig. 5 shows the finite element simulation temperature image of IGBT module chip layer under the working condition $\boldsymbol{w}$ = (1000W/(m^2·K), 200W), which means heat transfer coefficient h is 1000W/(m^2·K), and he total power loss Q is 200W. According to (11), the temperature field under this working condition is reduced by using the former r mode. When r = 1, 2, 3 and 4 are selected, the low-dimensional expressions of the original temperature field are shown in Fig. 6 respectively. It can be seen that with the increase of the number of selected modes r, the difference between the temperature field data restored by r modes and the original temperature field data becomes smaller and smaller. When r=4, the original temperature field data can be accurately restored by using the four modes, and the maximum and minimum values of temperature distribution are the same as the finite element simulation results.

It can be seen from Fig. 6 that the linear combination of r-dimensional feature vectors is used for approximate reduction of the original temperature field data. The approximate effects are different when the number of selected modes r is different. In (11), r = 1,2,3,4 are respectively selected for reduction of the original temperature field to calculate the average relative error

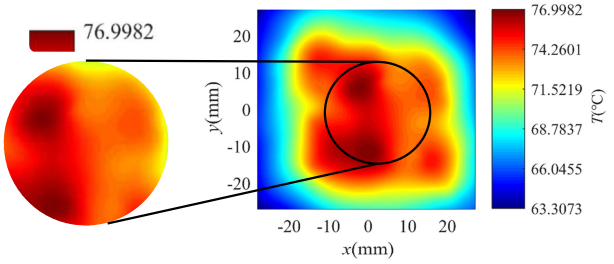

Fig. 5. Finite element simulation results($\boldsymbol{w}$ = (1000W/(m^2·K), 200W)).

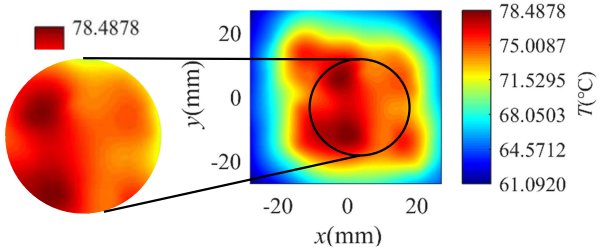

(a) 1 order model

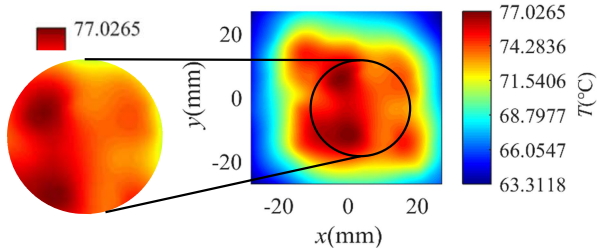

(b) 2 order model

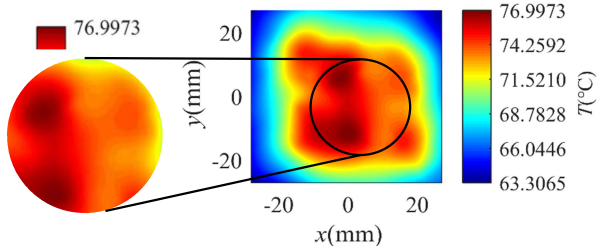

(c) 3 order model

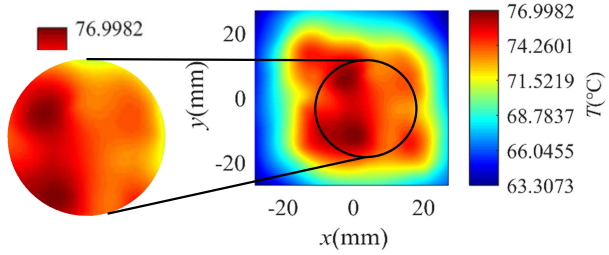

(d) 4 order model

Fig. 6. Calculation results of reduced-order model.

TABLE II
MEAN RELATIVE ERROR OF LOW DIMENSIONAL APPROXIMATION IN SAMPLE SPACE

r	1	2	3	4
Mean relative error (%)	1.56	7.56×10^{-2}	2.96×10^{-3}	1.34×10^{-10}

of the original temperature field data and the approximate temperature field data. Table II shows the calculation results.

As can be seen from Table II, when the selected modal number r increases, the calculation result of average relative error gradually decreases and the approximation effect of the original temperature field data improves.

B. Reduced-order Model Simulation Outside Sample Space

When the actual working conditions of the temperature field to be solved are different from those in the sample space (for example, $\boldsymbol{w}$ = (1250W/(m^2·K), 250W)), finite element simulation of IGBT is carried out. Fig. 7 shows the calculation results of the bottom temperature of the IGBT chip layer. In addition, the temperature field data under $\boldsymbol{w}$ = (1250W/(m^2·K), 250W) is calculated by the reduced-order model, and the temperature distribution of IGBT chip layer is obtained. When different mode numbers r = 1, 2, 3, and 4 are selected, the obtained results are shown in Fig. 8 respectively. By comparing the results of the reduced-order model with those of the finite element method, it can be seen that the results obtained by the two methods are basically same. With the increase of mode number r, the temperature field distribution obtained by the reduced-order model is closer to the finite element simulation results. When r = 4, the temperature field distribution obtained by the reduced-order model is basically consistent with the finite element simulation results, and the maximum and minimum temperature distribution are the same as the finite element simulation results.

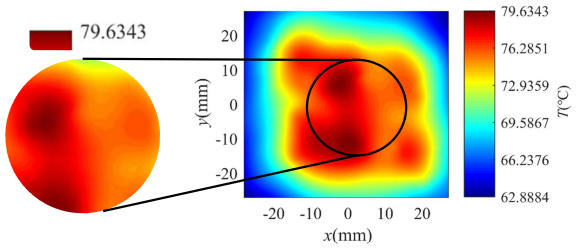

Fig. 7. Finite element simulation results($\boldsymbol{w}$ = (1250W/(m^2·K), 250W)).

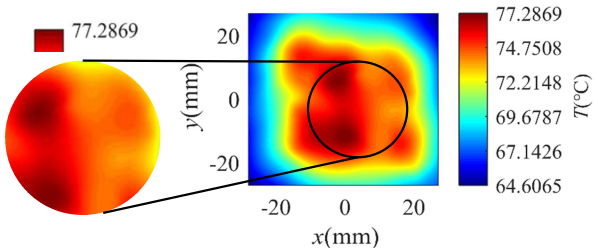

(a) 1 order model

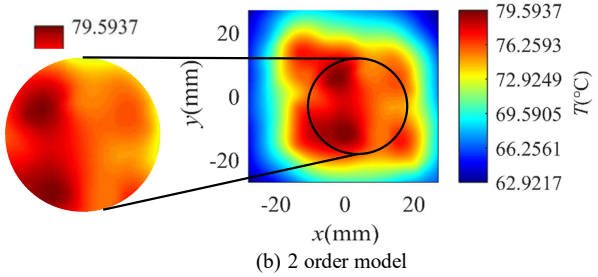

(b) 2 order model

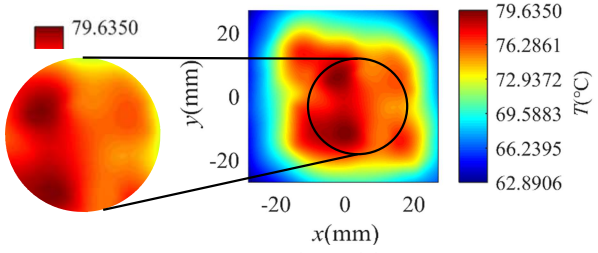

(c) 3 order model

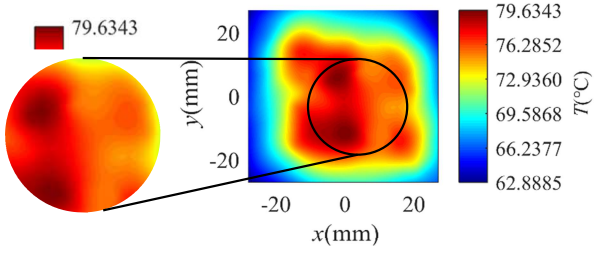

(d) 4 order model

Fig. 8. Calculation results of reduced-order model.

In order to evaluate the influence of the number of modes selected in the reduced-order model r on the solution accuracy of temperature field, different mode numbers r = 1,2,3,4 are selected under the condition of w = (1250W/(m2·K), 250W). Equations of different dimensions

are obtained by using the reduced-order model, and the temperature field is solved. The average relative error between the temperature field and the finite element simulation results is calculated, as in Table III.

TABLE III
THE AVERAGE RELATIVE ERROR OF THE RESULTS CALCULATED BY THE OUT-OF-SAMPLE SPACE REDUCED ORDER MODEL

r	1	2	3	4
Mean relative error (%)	1.79	6.54×10^{-2}	3.47×10^{-3}	1.60×10^{-4}

As can be seen from Table III, the larger the number of selected modes r is, the smaller the calculation error of the reduced-order model is. When mode 4 is selected, the calculation result of the reduced-order model is basically the same as the finite element calculation result.

C. Evaluation of Accuracy and Rapidity of Reduced-order Model

The reduced-order model is used to solve the temperature field under different working conditions, and the maximum value of the IGBT model temperature field is extracted, as in Fig. 9.The plane in Fig. 9 is the junction temperature upper limit that IGBT module can withstand, T_{vj}=175℃. The working conditions of IGBT module can be determined when the steady state temperature does not exceed the junction temperature upper limit.

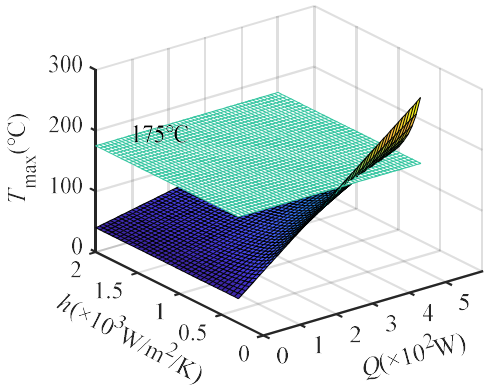

Fig. 9. Maximum temperature of IGBT module under different working conditions.

In order to evaluate the accuracy of the reduced-order model, the finite element simulation method and the numerical calculation method of the reduced-order model with 4 modes are used to solve the temperature field under different working conditions. Fig. 10 shows the calculated average error at each position. The heat transfer coefficient h ranges from 10W/(m^2·K) to 2000W/(m^2·K), and the total power loss ranges from 10W to 600W.It can be seen that the average error of the calculation results of the reduced-order model at each position increase with the decrease of the heat transfer coefficient H and the increase of the total power loss Q, and the average error is lower than 0.05553℃.

Considering the calculation error of the temperature field of the reduced-order model and the calculation result of the IGBT junction temperature, it can be found that the difference between the calculated result of the reduced-order model and

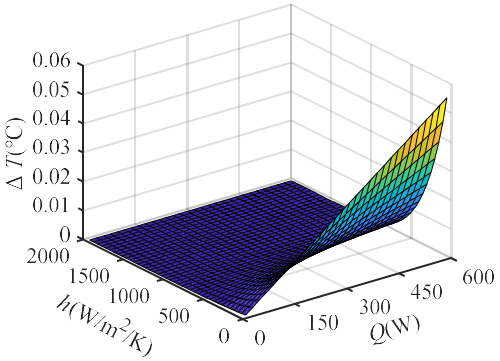

Fig. 10. The relative error of calculation results of reduced-order model.

that of the finite element is less than 0.1%, which indicates that the calculated result of the reduced-order model is accurate enough.

In order to evaluate the rapidity of the reduced-order model, the calculation time of the two solutions is determined and compared, as in Table IV.

TABLE IV
COMPARISON OF COMPUTING TIME BETWEEN DIFFERENT SOLVING MODELS

	Finite element model (refined mesh)	Finite element model (coarse mesh)	Reduced-order model
Time(s)	35	3	0.032814

The finite element model mesh contains 1028,522 degrees of freedom when the refined mesh element is used for section. The time required for a simulation solution is 35s.When the coarse mesh element is used for section, the finite element model grid contains 2770 degrees of freedom, and the time required for a simulation solution is 3s.After reducing the order of the finite element model with 2770 degrees of freedom, it takes 0.032814s for the model to perform a numerical calculation. By comparing the calculation time of several methods, it can be seen that the reduced-order model greatly reduces the time needed to solve the temperature field of IGBT module. When the original model is more complex and the degree of freedom is higher, the reduced-order model plays a more significant role in reducing the calculation time.

IV. CONCLUSION

Based on the finite element calculation of temperature field, the reduced-order model of IGBT module temperature field is proposed in this paper. Taking Infineon-FS200R07A5E3 IGBT of Infineon as an example, the simulation calculation and verification can be concluded as follows:

(1) The sample space of temperature field can be approximated in low dimension according to the relative energy of the modes. The characteristic of the relative energy of the first several modes is much larger than that of the other remaining modes. For the research object adopted in this paper, it is better to adopt the first four modes approximation

(2) The results of temperature field calculation show that the accuracy of the results can be guaranteed by the results of the reduced-order equations under different working conditions, and the error between the results of temperature field

calculation and the finite element results is less than 0.1%.

(3) Compared with the finite element model, the calculation time of the reduced-order model is greatly reduced. In this paper, the calculation time of the finite element model can be accelerated from 3s to 0.03s.

REFERENCES

[1] S. Yang, A. Bryant, P. Mawby, D. Xiang, L. Ran and P. Tavner, "An Industry-Based Survey of Reliability in Power Electronic Converters," *IEEE Trans. Industry Applications*, vol. 47, no. 3, pp. 1441-1451, May-June 2011.

[2] L. R. GopiReddy, L. M. Tolbert and B. Ozpineci, "Power Cycle Testing of Power Switches: A Survey," *IEEE Trans. Power Electronics*, vol. 30, no. 5, pp. 2465-2473, May 2015.

[3] L. Dupont, Y. Avenas and P. Jeannin, "Comparison of Junction Temperature Evaluations in a Power IGBT Module Using an IR Camera and Three Thermosensitive Electrical Parameters," *IEEE Trans. Industry Applications*, vol. 49, no. 4, pp. 1599-1608, July-Aug. 2013.

[4] M. Berthou, P. Godignon and J. Millán, "Monolithically Integrated Temperature Sensor in Silicon Carbide Power MOSFETs," *IEEE Trans. Power Electronics*, vol. 29, no. 9, pp. 4970-4977, Sept. 2014.

[5] Y. Zhang, E. Deng, Z. Zhao, J. Chen, S. Fu and X. Cui, "Experimental Verification of the Junction Temperature Distribution within Press Pack IGBTs," 2020 32nd International Symposium on Power Semiconductor Devices and ICs (ISPSD), 2020, pp. 360-363

[6] T. Li, X. Du, C. Zeng, P. Sun and H. Tai, "A Quasi-online Method of Thermal Network Parameter Identification for IGBT Modules," 2016 IEEE Energy Conversion Congress and Exposition (ECCE), 2016, pp. 1-6

[7] Y. Zhou et al., "Dynamic junction temperature estimation via built-in negative thermal coefficient (NTC) thermistor in high power IGBT modules," 2017 IEEE Applied Power Electronics Conference and Exposition (APEC), 2017, pp. 772-775

[8] Z. Wang and W. Qiao, "A Physics-Based Improved Cauer-type Thermal Equivalent Circuit for IGBT Modules," *IEEE Trans. Power Electronics*, vol. 31, no. 10, pp. 6781-6786, Oct. 2016

[9] B. Ji, V. Pickert, W. Cao and B. Zahawi, "In Situ Diagnostics and Prognostics of Wire Bonding Faults in IGBT Modules for Electric Vehicle Drives," *IEEE Trans. Power Electronics*, vol. 28, no. 12, pp. 5568-5577, Dec. 2013.

[10] Aquino, W. "An Object-oriented Framework for Reduced-order Models Using Proper Orthogonal Decomposition (POD)." *Computer Methods in Applied Mechanics & Engineering*, vol. 196, no. 41-44, pp. 4375-4390, May. 2007.

[11] Benjamin, P., W. Karen, and G. Max, "Survey of Multifidelity Methods In Uncertainty Propagation, Inference, And Optimization." *SIAM Review*, vol. 60, no. 3, pp: 550-591, 2018.

[12] A, David J. Lucia, P. S. B. B, and W. A. S. C. "Reduced-order Modeling: New Approaches For Computational Physics," *Progress in Aerospace Sciences*, vol. 40, no. 1-2, pp. 51-117, 2004.

[13] M. Ma et al., "A Three-Dimensional Boundary-Dependent Compact Thermal Network Model for IGBT Modules in New Energy Vehicles," *IEEE Trans. Industrial Electronics*, vol. 68, no. 6, pp. 5248-5258, June 2021.

[14] Miner M A. *Journal of Applied Mechanics*, 1945, pp: A159-A164.s

[15] A. D. Rajapakse, A. M. Gole and P. L. Wilson, "Electromagnetic Transients Simulation Models for Accurate Representation of Switching Losses and Thermal Performance in Power Electronic Systems," *IEEE Trans. Power Delivery*, vol. 20, no. 1, pp. 319-327, Jan. 2005.

Ziyu Zhou was born in China on April 1998. He received the B.E. and M.E. degree in electrical engineering from Harbin Institute of Technology, Harbin, China, in 2020 and 2022, respectively. He is currently working toward the Ph.D. degree in the School of electrical engineering from Harbin Institute of Technology, Harbin, China. His current research interests include design, control and analysis of permanent-magnet synchronous machines system.

Yi Sui (Member, IEEE) was born in Jilin, China, in 1987. He received the B.Sc., M.Sc., and Ph.D. degrees in electrical engineering from the Harbin Institute of Technology, Harbin, China, in 2009, 2011, and 2016, respectively.

Since 2016, he has been with Harbin Institute of Technology, where he has been a Professor since 2021.

His current research interests include fault-tolerant permanent-magnet synchronous machines and permanent-magnet linear machines.

Xu Zhang was born in China on September 1997. She received the B.E. and M.E. degree in electrical engineering from Harbin Institute of Technology, Harbin, China, in 2019 and 2021, respectively. She is currently working as an engineer in Huawei Technologies Co., Ltd, Dongguan, China. Her current research interests include design and development of battery management system in energy storage applications.

Chengde Tong (Member, IEEE) received the B.Sc., M.Sc., and Ph.D. degrees in electrical engineering from the Harbin Institute of Technology, Harbin, China, in 2007, 2009, and 2013, respectively.

He is currently a Professor with the Department of Electrical Engineering, Harbin Institute of Technology. He is the author or a coauthor of more than 60 published articles.

His research interests include electric drives and energy management of hybrid electric vehicles, control of free-piston Stirling and internalcombustion engines, and permanent-magnet linear machines.

Ping Zheng (Senior Member, IEEE) received the B.Sc., M.Sc., and Ph.D. degrees from the Harbin Institute of Technology, Harbin, China, in 1992, 1995, and 1999, respectively, all in electrical engineering.

Since 1995, she has been with Harbin Institute of Technology, where she has been a Professor since 2005. She is the author or coauthor of more than 270 published refereed technical papers and four

books. She is the holder of 70 Chinese invention patents. Her current research interests include electric machines and control, hybrid electric vehicles, and the cloud computing of electric machine system.

Dr. Zheng was a recipient of more than 30 technical awards, including the “China Youth Science and Technology Award” from the Organization Department of the Communist Party of China in 2009, the “National Science Foundation for Distinguished Young Scholars of China” from the National Natural Science Foundation of China in 2013, the “Chang Jiang Scholar Professor” from the Ministry of Education of China in 2014, and the “National High-Level Talent Special Support Program” from the Organization Department of the Communist Party of China in 2016.

Mingjun Zhu was born in China on May 1988. He received the B.E. and M.E. degree in electrical engineering from Northwestern Polytechnical University and Harbin Institute of Technology, China, in 2011 and 2013, respectively. Since 2013, he has been a Senior Engineer with Xi'an Flight Automatic Control Research Institute, Xi'an, China. His current research interests include control and analysis of permanent magnet synchronous machines system and EHA design.